GLOBAL BIOGEOCHEMICAL CYCLES, VOL. 15, NO. 1, PAGES 81-99, MARCH 2001

Potential impact of climate change on marine export production

Laurent Bopp,[1] Patrick Monfray,[1] Olivier Aumont,[1] Jean-Louis Dufresne,[2] Hervé Le Treut,[2] Gurvan Madec,[3] Laurent Terray,[4] and James C. Orr[1]

Abstract. Future climate change will affect marine productivity, as well as other many components of Earth system. We have investigated the response of marine productivity to global warming with two different ocean biogeochemical schemes and two different atmosphere-ocean coupled general circulation models (GCM). Both coupled GCMs were used without flux correction to simulate climate response to increased greenhouse gases (+1% CO_2/yr for 80 years). At 2xCO_2, increased stratification leads to both reduced nutrient supply and increased light efficiency. Both effects drive a reduction in marine export production (-6%), although regionally changes can be both negative and positive (from -15% zonal average in the tropics to +10% in the Southern Ocean). Both coupled models and both biogeochemical schemes simulate a poleward shift of marine production due mainly to a longer growing season at high latitudes. At low latitudes, the effect of reduced upwelling prevails. The resulting reduction in marine productivity, and other marine resources, could become detectable in the near future, if appropriate long-term observing systems are implemented.

1. Introduction

Much effort has been devoted to address how climate will change due to emissions of greenhouse gases and aerosols. Although large uncertainties still remain, particularly concerning cloud response, all atmospheric general circulation models (GCM) simulate future global warming if emissions of greenhouse gases continue unabated. Previous studies with ocean GCMs have demonstrated that such climate change will also affect ocean circulation. To include such ocean feedback on climate, recent studies have used coupled atmosphere-ocean GCMs. Coupled models converge to a global warming and simulate that Earth's surface warms by 1°- 3°C when atmospheric CO_2 reaches twice its preindustrial concentration [*Houghton et al.*, 1996]. Coupled GCMs also simulate that the ocean thermohaline circulation becomes more sluggish. Formation of North Atlantic Deep Water (NADW) is reduced and may even collapsed entirely at 4xCO_2 [*Manabe et al.*, 1991]. Additionally, the upper ocean becomes globally more stratified owing to increases in surface temperature and precipitation [*Manabe et al.*, 1991; *Manabe and Stouffer*, 1993; *Sarmiento et al.*, 1998].

How such physical changes will affect marine productivity is poorly understood. Any such changes would obviously propagate up to the marine foodweb. For instance, interannual variations in marine productivity due to El Niño have dramatically affected ocean fisheries yields and the human populations that rely on them worldwide. Previous modeling studies have contented themselves with focusing on how large climate-induced changes could alter the ocean carbon cycle and atmospheric CO_2 [*Maier-Reimer et al.*, 1996; *Sarmiento and Le Quéré*, 1996; *Sarmiento et al.*, 1998; *Joos et al.*, 1999; *Matear and Hirst*, 1999]. The ocean carbon-cycle models (OCCM) used for these studies were necessarily simplistic. They used phosphorus-only based schemes, either prognostically [*Maier-Reimer et al.*, 1996; *Joos et al.*, 1999; *Matear and Hirst*, 1999] or diagnostically, restoring to present-day observed surface phosphates [*Sarmiento and Le Quéré*, 1996; *Sarmiento et al.*, 1998]. These models simulate biogeochemical fluxes but do not include explicit plankton dynamics.

[1]Institut Pierre-Simon Laplace/Laboratoire des Sciences du Climat et de l'Environnement, Gif sur Yvette, France.

[2]Institut Pierre-Simon Laplace/Laboratoire de Météorologie Dynamique, Jussieu, Paris.

[3]Institut Pierre-Simon Laplace/Laboratoire d'Océanographie Dynamique et de Climatologie, Jussieu, Paris.

[4]Centre Européen de Recherche et de Formation Avancée pour le Calcul Scientifique, Toulouse, France.

Paper number 1999GB001256.
0886-6236/01/1999GB001256$12.00

In contrast to previous studies, our focus is not on ocean and atmospheric carbon. Instead, our interest is on predicting the regional and global effects of climate change on marine productivity. First we use a prognostic geochemical model, similar to previous studies [*Maier-Reimer et al.*, 1996; *Matear and Hirst*, 1999]. Second, as a measure of reliability, we use a more sophisticated biogeochemical model that includes explicit phytoplankton dynamics.

2. Models and Simulations

2.1. Climate Models

Our biogeochemical simulations were conducted offline. That is, we used archived oceanic fields of advection and eddy diffusion, predicted from two different coupled atmosphere-ocean GCMs, each of which used the same ocean model. Coupled simulations were made in the context of the Coupled Model Intercomparison Project II (CMIP II) of World Climate Research Programme/Climate Variability and Predictability Programme (WCRP/CLIVAR). With each coupled model, we made two different climate simulations. The first simulation consists of a control climate, in which atmospheric pCO_2 was kept constant at 350 ppm. The second simulation is a global warming scenario in which atmospheric pCO_2 was increased from 350 ppm at a rate of 1% yr^{-1}, until it reached $2xCO_2$ (700 ppm) after 70 years (Table 1a).

Both coupled GCMs use the same ocean model, Océan Parallélisé Ice (OPAICE) [*Madec et al.*, 1997]. That ocean model is original for two principal reasons. First it solves the primitive equations on a curvilinear grid [*Madec and Imbard*, 1996], whose resolution averages 2^o longitude by 1.5^o latitude. Meridional resolution is higher at the equator (0.5^o) to take into account its enhanced dynamics. Vertically, the grid has 30 levels, 10 are in the first 100 m; the deepest layer is 500 m thick and reaches 5000 m. Second, vertical diffusion and viscosity coefficients are computed prognostically using a 1.5 turbulent closure scheme [*Blanke and Delecluse*, 1993], which describes turbulent kinetic energy (TKE) throughout the water column from surface heat fluxes and wind stress as well as water column stability. Therefore OPAICE predicts turbulence both in and below the mixed layer. Thus the mixed layer depth varies in time. Furthermore, OPAICE uses an isopycnal parameterization of lateral diffusivity but without horizontal background diffusivity [*Lazar et al.*, 1999]. Finally, OPAICE includes a simple sea-ice model taking into account the relevant thermodynamical processes concerning snow and ice transformations [*Filiberti et al.*, 1999].

The oceanic and atmospheric components of each CGCMs are coupled through the coupler Ocean Atmosphere Soil Interface Software (OASIS) [*Terray et al.*, 1999]. The function of this module is to ensure time synchronization of the atmospheric and oceanic components and to perform spatial interpolation of the coupled fields between the different atmospheric and oceanic grids. Coupled simulations are made without flux correction.

Table 1a. Climate Simulations

Run[a]	Experiment	Climate Model
Lc	Control	LMD/OPAICE
Ls	Scenario	LMD/OPAICE
Ac	Control	ARPEGE/OPAICE
As	Scenario	ARPEGE/OPAICE

[a]L for LMD/OPAICE, A for Arpege/OPAICE, c for control run (pCO_2 = 350ppm), s for scenario run (1% yr^{-1} increase in atmospheric pCO_2).

The two coupled GCMs differ only in their atmospheric component. The first coupled model (L, Table 1a), uses the atmospheric model of the Laboratoire de Météorologie Dynamique, version 5 (LMD5) [*Sadourny and Laval*, 1984]. This LMD5 model uses a finite difference numerical scheme. The horizontal grid has a longitudinal resolution of 5.6^o; latitudinally, resolution varies with the sine of the latitude. LMD5 has 15 vertical layers.

The second coupled model (A, Table 1a) from *Guilyardi and Madec* [1997] uses the atmospheric model Arpege (Climat Version 2) from Météo-France [*Déqué et al.*, 1994]. The Arpege model is a climatic spectral atmosphere model based on the Arpege weather forecast model. Its horizontal grid is based on a triangular spectral T31 truncation, which corresponds to a grid size of 3.75^o. Arpege has 19 vertical layers including 3 layers in the stratosphere.

2.2. Biogeochemical Schemes

As a reference biogeochemical scheme, we use the Hamburg ocean carbon cycle model (HAMOCC3), a simple prognostic model based on phosphates [*Maier-Reimer*, 1993]. In fact, HAMOCC3 is not truly a biogeochemical model. Although it models geochemical fluxes, it contains no explicit biology. We will refer to this scheme as G, for geochemical (Table 1b). The G scheme was implemented by *Aumont et al.* [1999] within our ocean model. The G scheme links marine export production (EP) to phosphate utilization in the upper 50 m through the following equation:

$$\mathrm{EP} = r_0\, I\, \frac{T + 2^{\circ}\mathrm{C}}{T + 10^{\circ}\mathrm{C}}\, \frac{50}{Z_m}\, \frac{{\mathrm{PO_4}}^2}{P_0 + \mathrm{PO_4}}, \qquad (1)$$

where EP is defined as the part of the particulate or-

Table 1b. Biogeochemical Simulations

Biogeochemical Run [a]	Biogeochemical Scheme	Climate Forcing
LGc	HAMOCC3	Lc
LGs	HAMOCC3	Ls
LBc	P3ZD	Lc
LBs	P3ZD	Ls
AGc	HAMOCC3	Ac
AGs	HAMOCC3	Ls

[a] G for Geochemical scheme (HAMOCC3); B for Biogeochemical scheme (P3ZD).

ganic carbon produced in the euphotic zone that is transported out of the first 100 meters; PO_4 is the mean phosphate concentration in the upper 50 m, $P_0 = 0.02$ μmol L^{-1}, Z_m is the mixed layer depth, T is the temperature, I is an incoming radiation coefficient (whose ranges from 0 to 1), and r_0 is the maximum productivity rate (0.25 month^{-1}). The term $50/Z_m$ approximates the inhibition of light utilization by turbulence. It is applied only when the mixed layer depth is greater than the euphotic zone depth (here 50 m). If the mixed layer is shallower than 50 m, that term is set equal to 1; that is, no light efficiency reduction is applied. Below 100 m, the production is exported and remineralized instantaneously according to an empirical power law function derived from measured fluxes from sediment traps [*Suess*, 1980]. This G scheme, coupled to OPA (Océan Parallélisé), has been validated both for the seasonal cycle of biogeochemical tracers [*Aumont*, 1998] and for the interannual variability of carbon fluxes to the ocean [*Le Quéré et al.*, 2000].

Our second biogeochemical scheme is more true to that term since it explicitly includes plankton dynamics. We refer to it as the B scheme, B for biogeochemical (Table 1b). More specifically, we use the P3ZD model from *Aumont* [1998], an nutrient phytoplankton zooplankton and detritus (NPZD) type model that includes five reservoirs: phosphate, phytoplankton, zooplankton, dissolved organic matter, and particulate organic matter. A similar scheme was previously included in the Hamburg global OCCM [*Six and Maier-Reimer*, 1996]. *Aumont et al.* [2000] detail the B scheme we use here. Both explicit prognostic schemes provide a more realistic seasonal cycle of marine productivity and large-scale transport of nutrients from upwelling areas to oligotrophic gyres. This B scheme computes explicitly the penetration of light into the photic zone. Phytoplankton growth depends on the local conditions of light, temperature, and vertical eddy diffusion, which acts to homogenize the concentration of phytoplankton cells throughout the complete mixed layer. Additionally, the B scheme allows us to explicitly diagnose chlorophyll content. For that we use the relationship of *Doney et al.* [1996] to compute the C/Chl ratio of phytoplanktonic cells. The B scheme considers only one class of zooplankton, which feeds on both phytoplankton and particulate organic carbon (POC). In the top 100 m of the water column, POC is assumed to sink at a constant rate (5 m d^{-1}). Some of these particles reach 100 m depth and thereby contribute to particulate export production as defined for this paper. Subsequently, these particles are exported instantaneously to depth following the same empirical profile used in the G scheme.

2.3. Carbon-Climate Simulations

Practically, to reduce CPU requirements and make our simulations feasible, we chose to use an off-line tracer-transport version of the OPA ocean circulation model. We coupled that ocean model with each of our biogeochemical schemes. Thus our off-line experiments were driven by archived monthly average fields of advection and vertical turbulent diffusion from each of the two dynamic coupled atmosphere-ocean models. We made three pairs of simulations (Table 1b): the G scheme was coupled to the L and A models (LG and AG models), and the B scheme was coupled to the L model (LB model). Simulations were initialized with the final steady state tracer distribution of *Aumont et al.* [1999].

3. Results

3.1. Climate Runs

3.1.1. Control runs. The climate of our two control simulations, one with each coupled model (Lc and Ac), remains stable over the duration of the simulation (80 years) [*Barthelet et al.*, 1998a,b]. The overall atmospheric and oceanic circulations simulated in both control simulations are generally consistent with modern observations and thus capture the gross features of the present-day climate. However, differences between simulated sea surface temperature (SST) at the end of the control simulations and the present-day SST [*Levitus*, 1982] show some systematic biases. The Lc SSTs are too warm in the Southern Ocean and too cold in the tropics; the Ac SSTs are too warm in the

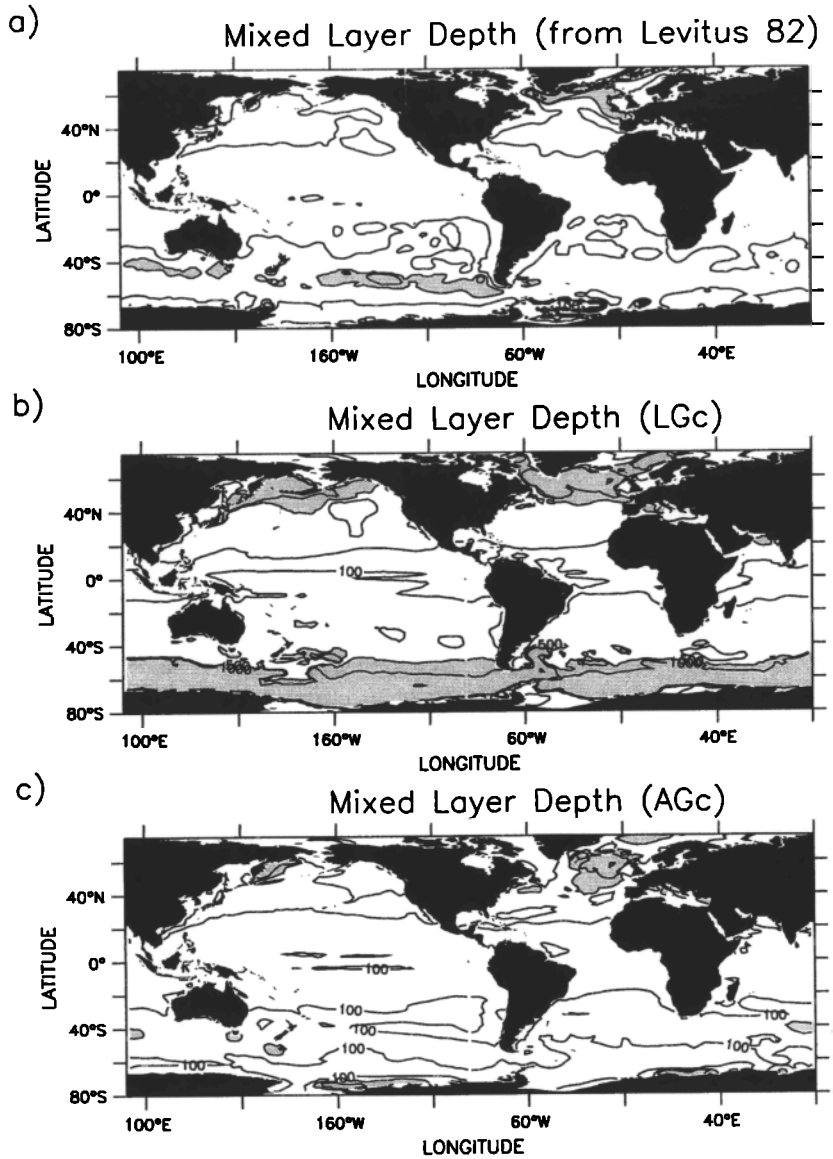

Figure 1. Maximum mixed layer depth (wintertime) from (a) the climatologies and control simulations for the (b) L and (c) A models. Shaded areas indicate regions where the mixed layer depth exceeds 500 m. The criterion used in our model simulations is based on the predicted vertical diffusion coefficient and differs from that used here for the climatologies (a difference of 0.125 kg m^{-3} in density relative to the surface).

eastern tropics, subtropics, and in the Southern Ocean. The Southern Ocean is too warm in both CGCMs, and Antarctic sea-ice cover is inadequate. Generally though, deep water formation appears adequate in the Greenland and Norwegian seas, as well as around Antartica: in Ac both NADW and AABW form at a rate of 16 Sv, in Lc, deep-water formation is much stronger, perhaps too strong (nearly 30 Sv for NADW and 34 Sv for AABW in Lc control simulation).

A principal difference between Ac and Lc control runs concerns the predicted mixed layer depth. Figure 1 compares the maximum of the mixed layer depth predicted in both dynamical models to estimates from *Levitus* [1982] climatologies. In Lc the mixed layer depth is generally too deep, particularly in the Southern Ocean (Figure 1) where it often extends beyond 1000 m. On the contrary, in Ac, the mixed layer depth in the polar frontal zone of the Southern Ocean is too shallow (less than 600 m deep in Ac versus greater than 1000 m as estimated from the observations). The difference between Ac and Lc in the Southern Ocean must be explained by differences in the atmospheric component of the two coupled models: in Lc, summer precipitation is inadequate, in Ac, loss of heat from the Southern Ocean is

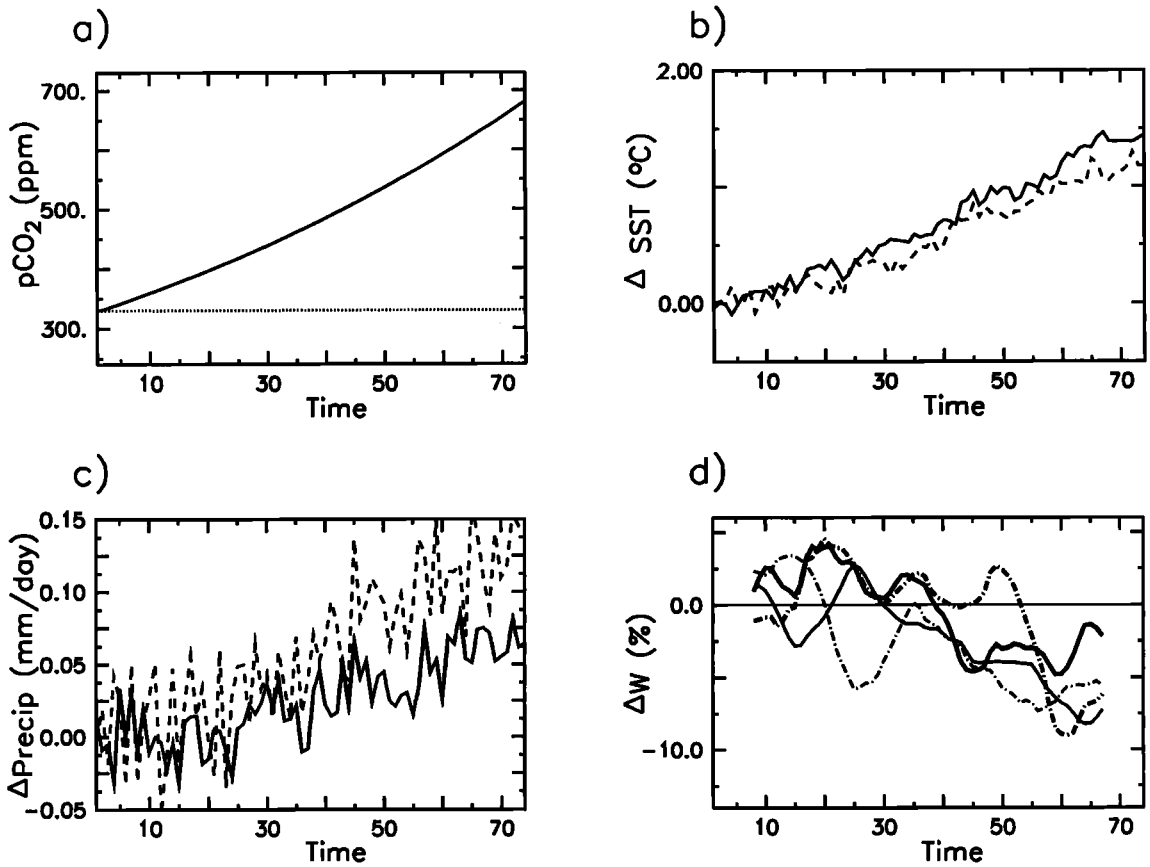

Figure 2. Time series of (a) atmospheric CO_2 (ppm) which is constant for the control simulations (dotted line) but increases at a rate of 1% yr^{-1} for global warming simulations (dashed line), (b) the global mean SST difference between global warming and control runs (A (dashed line); L (solid line)), (c) the corresponding global difference in mean precipitation over the ocean, and (d) the relative change in upwelling velocity (upward) accross 50 m, for L in the equatorial Pacific (thin, solid lines) and off coastal Peru and Chile (thin, dot-dashed lines), as well as A in the same regions (thicker lines, same patterns).

inadequate. The North Pacific is another region where both models fail to reproduce a realistic mixed layer. In that region, both models produce a mixed layer that is too deep as well as excessive deep water formation.

3.1.2. Global warming runs. Both global warming simulations (As and Ls) showed substantial change relative to their control runs (Ac and Lc) [*Barthelet et al.*, 1998a,b]. Most notable were increases in SST (Figure 2b) and near-surface ocean stratification, owing both to warming and increased precipitation (Figure 2c). At $2xCO_2$ (years 65-75), global average surface warming reached +1.5°C for Ls-Lc and +1.2°C for As-Ac. Both estimates fall within the range of other CMIP models (1°-3°C). The increase in precipitation over the ocean during the last decade of integration was +2-3% for Ls-Lc and +3-4% for As-Ac.

Increased temperature in the tropics and increased rainfall in the high and middle latitudes cause a reduction of surface density from pole to pole in both models (Figures 3a and 3b). This increased surface buoyancy resulted in a general stratification of the surface ocean, with a pattern that is surprisingly similar in both L and A models (Figure 3c). However, the mixed layer depth shoals considerably more in the Southern Ocean in L relative to A. This difference is that in the control runs, the mixed layer is much deeper and has more potential for change, in Lc relative to Ac (Figure 1). Interestingly, the As-Ac difference shows the opposite trend, a deepening of the mixed layer, south of 70°S. This deepening is generated by the gradual disappearance of the Antarctic sea ice cover and the opening up of new areas of deep convective mixing.

Global warming also affected the subsurface and deep ocean: changes in sea surface temperature and salinity drove reductions in NADW formation of about -13% in both models (-4 Sv in Ls-Lc and -2 Sv in As-Ac). AABW was also reduced in both models (about -3 Sv in Ls-Lc, which is a 10% decrease). These changes were

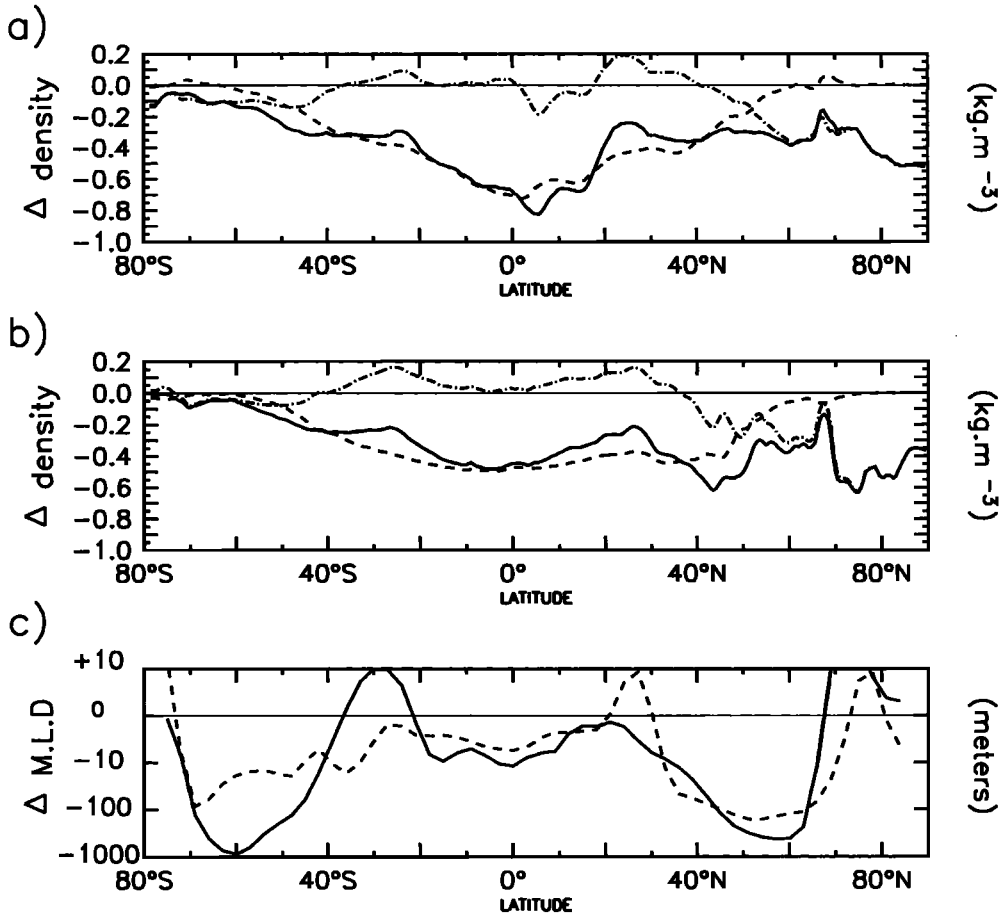

Figure 3. Zonal mean change in surface density (in $kg\,m^{-3}$) including the total change (solid line), the change due to temperature (dashed line) and the change due to salinity (dot-dashed line) for (a) the L model, (b) the A model, and (c) corresponding changes in mixed layer depth (m, log-scale) for L (solid line) and A (dashed line) models.

driven by warming and freshening in the high-latitude surface waters. The freshening was driven both by increased precipitation and ice melt, owing to general warming.

Finally, both coupled models predict a reduction in the intensity of coastal and equatorial upwellings. Figure 2d shows the relative changes in upwelling intensity for the equatorial Pacific and off the coast of Peru and Chile. This reduction is linked to a decline in the trade wind intensity.

3.2. Biogeochemical Control Runs

The control climate simulations (AGc, LGc, and LBc) were evaluated by comparing simulated PO_4^{3-} and particulate export production to available data. For the LB model, we were also able to evaluate, on a global scale, by comparing simulated surface chlorophyll to that derived by remote sensing.

3.2.1. Phosphate. Simulated surface PO_4^{3-} (Figure 4) shows similar patterns as the observations [*Levitus et al.*, 1993]: high concentrations are found near the poles and in upwelling areas, and low concentrations are found in the subtropical gyres. However, simulated PO_4^{3-} differs from observations in several key regions. In the Southern Ocean, PO_4^{3-} concentrations appear very sensitive to vertical mixing: in AGc, vertical mixing is weak, and surface concentrations are much too low; in LGc and LBc, vertical mixing is stronger, and PO_4^{3-} concentrations are more realistic. Yet we do not mean to imply here that vertical mixing in the Southern Ocean in Lc is more realistic. Other factors also enter in, in this high-nutrient low-chlorophyll (HNLC) region, such as limitation by iron [*Martin et al.*, 1987], which are not included in our models. In the subtropical gyres, all three models predict lower PO_4^{3-} concentrations than observed. Conversely, in the North Pacific, all models simulate a local maximum in surface PO_4^{3-} roughly as observed, despite unrealistic vertical mixing. The lack of that maximum has been a problem with previous studies [*Maier-Reimer*, 1993; *Six and Maier-*

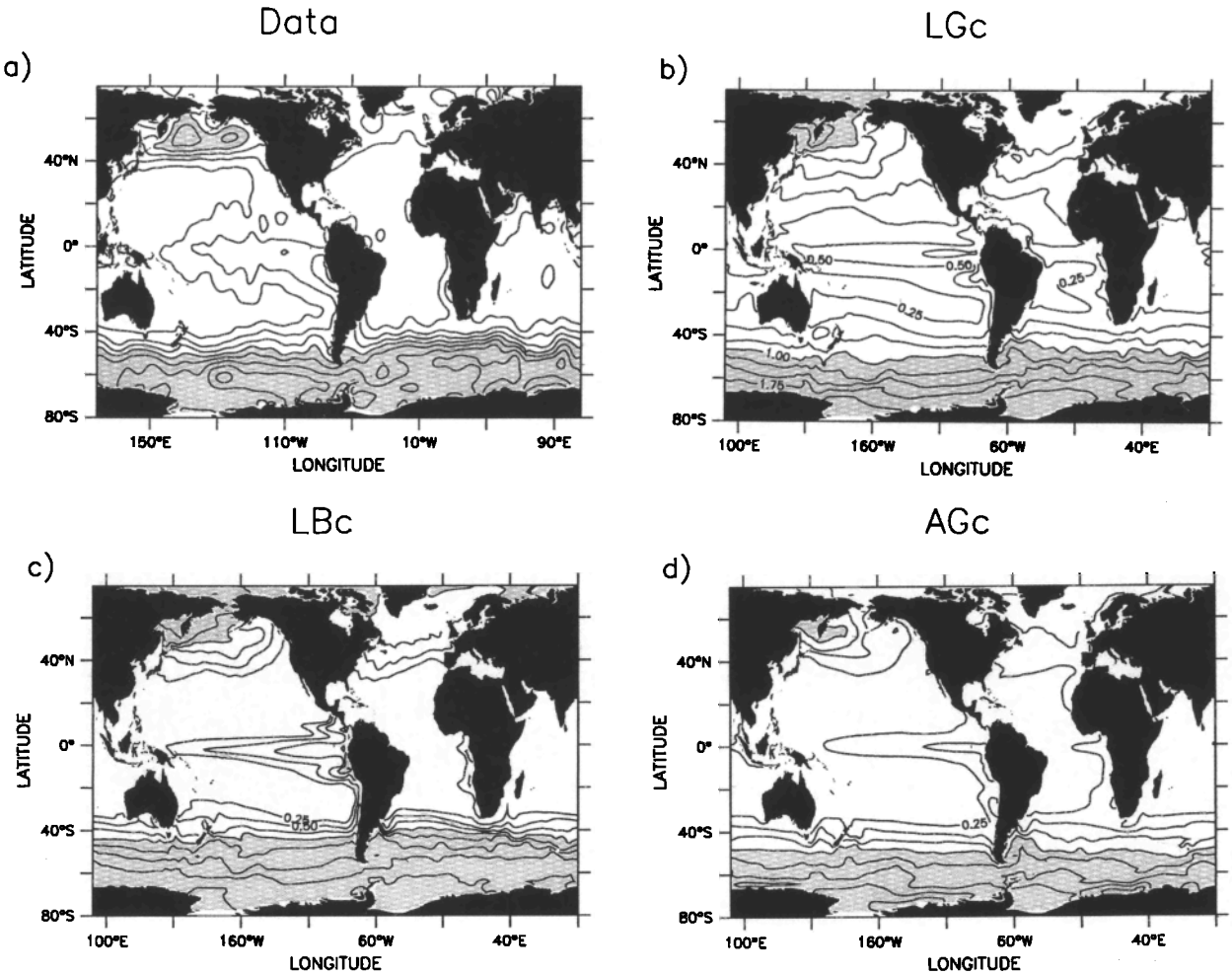

Figure 4. Surface PO_4^{3-} (in μmol L^{-1}) (a) observed and modeled by (b) LGc, (c) LBc, and (d) AGc. The contour interval is 0.25 μmol L^{-1} and shaded areas denote surface concentrations higher than 1 μmol L^{-1}.

Reimer, 1996; *Yamanaka and Tajika*, 1996]. Nonetheless, this maximum is too weak and too far to the west of North Pacific, in our models, owing to a poor representation of the ocean dynamics in this region.

3.2.2. Chlorophyll. Data obtained from remote sensing by NASA's Sea-viewing Wide Field-of-view Sensor (SeaWiFS) provide the means to validate the models surface distribution of chlorophyll at the global scale. Yet this validation effort could only be applied to our LBc simulation because only our B scheme can be used to diagnose chlorophyll content. Plate 1 shows the simulated and satellite-derived distributions of chlorophyll at the surface for May and November. Globally, the simulated patterns generally match those which are observed Concentrations below 0.1 mg Chl m^{-3} are found in the oligotrophic gyres both in the model and the observations. In the high latitudes of the Northern Hemisphere, the model reproduces the seasonal variability of chlorophyll suggested by the satellite observations and in situ measurements at NABE (North atlantic Bloom Experiment) and India stations in the North Atlantic In the equatorial Pacific ocean, the predicted chlorophyll concentrations are largely overestimated, both in May and November. Observations show concentrations of $\sim$ 0.1-0.3 mg Chl m^{-3}, while in the model they exceed 0.4 mg Chl m^{-3}. However, the equatorial Pacific is an HNLC region. In situ experiments have demonstrated that biological activity is indeed iron limited in that region [*Coale et al.*, 1996]. Another study suggests that phytoplankton growth may also be limited by the availability of silicate in this region [*Dugdale and Wilkerson*, 1998]. Our B scheme does not include such limitations. This may explain why the B scheme clearly overestimates chlorophyll in this region. In other HNLC regions (North Pacific, Southern Ocean), LBc also exhibits the same defaults. In the North Pacific, LBc predicts values which are too high. In the Southern Ocean, LBc simulates both a strong seasonality and a large spa-

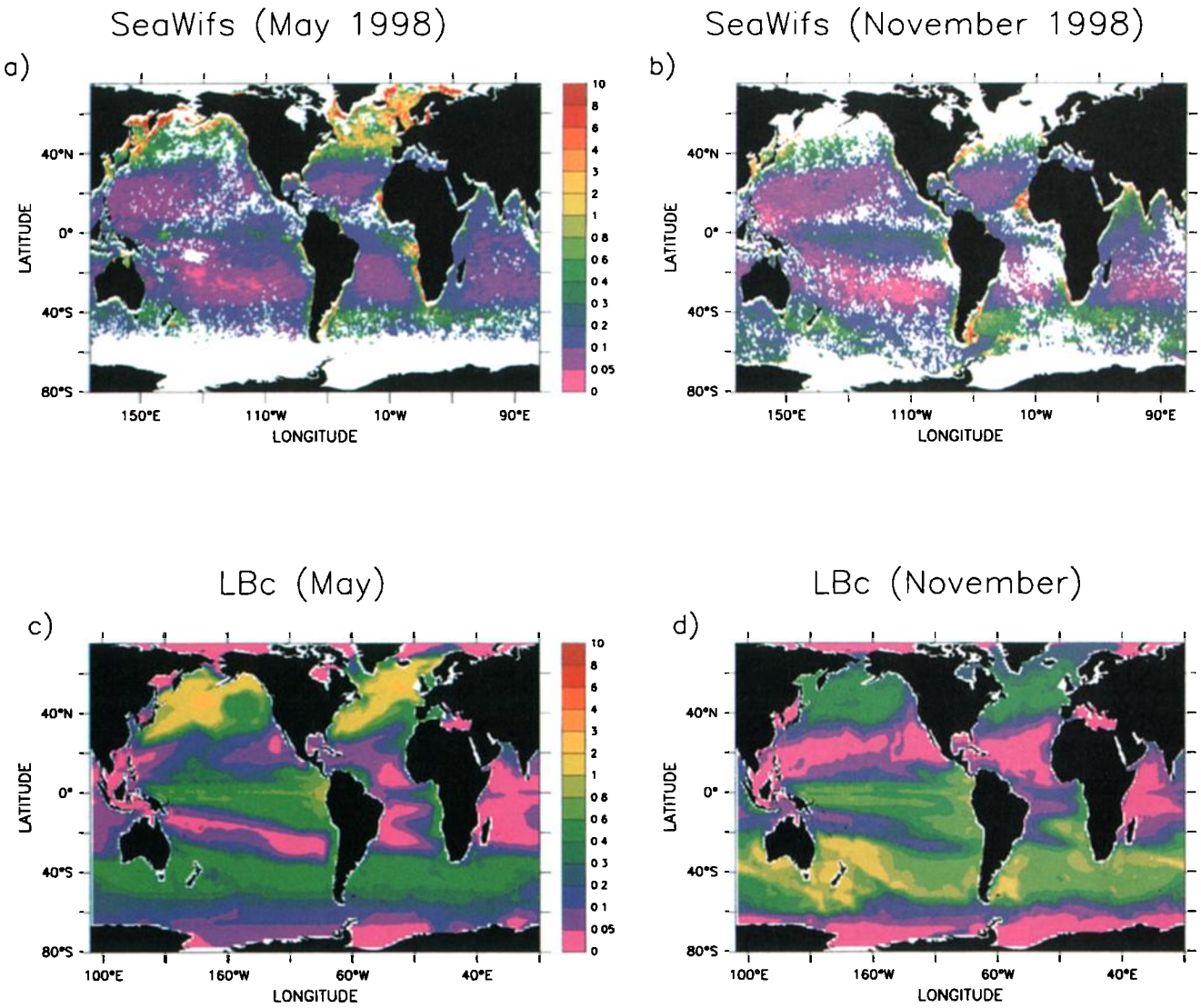

Plate 1. Surface chlorophyll (in mg m^{-3}) derived from remote sensing (SeaWiFS) for (a) May 1998 and (b) November 1998, compared to simulated chlorophyll from LBc (c) May, and (d) November.

tial heterogeneity, similar to the observations, but simulated chlorophyll is too high, especially in November (up to 2 mg Chl m^{-3} in the model versus less than 1 mg Chl m^{-3} observed).

3.2.3. Export production. We define particulate export production EP at 100 m as that part of the primary production that is transported below 100 m. Simulated EP is 13.1 GtC yr^{-1} in LGc, 9.5 GtC yr^{-1} in AGc, and 11.1 GtC yr^{-1} in LBc. These global estimates fall in the range of POC export production estimated from observations (3.5-20 GtC yr^{-1}) [*Berger and Wefer*, 1991; *Jahnke*, 1996] as well as that from simulations with other global carbon cycle models (8.5-15 GtC yr^{-1}) [*Najjar et al.*, 1992; *Anderson and Sarmiento*, 1995; *Yamanaka and Tajika*, 1996; *Six and Maier-Reimer*, 1996]. Our B scheme is novel because it explicitly computes the primary production. In LBc, the total primary production is estimated to 64.7 GtC yr^{-1}, which is near the upper limit of previous estimates [*Martin et al.*, 1987; *Antoine et al.*, 1996].

Our zonal mean of export production is compared to estimates derived from remote sensing of ocean color (Figure 5). To make this comparison we first exploit the primary production that was computed from the CZCS ocean color archive [*Antoine et al.*, 1996; *Balkanski et al.*, 1999]. Then, we use a simple algorithm [*Berger and Wefer*, 1991] to compute the *f* ratio and derive the export production. Within the large uncertainties associated with such a derivation, export production derived from the observations are generally consistent with that simulated by our three models (Figure 5). In the Southern Ocean though, export production simulated in LGc and AGc is much larger than derived estimates. Conversely, much better agreement is found with simulation LBc, with its more sophisticated biogeochemistry.

Regionally, LGc and AGc show similar patterns of export production (Plate 2). The simple phosphate-based G scheme used in these two models causes export production to closely follow surface PO_4^{3-} concentrations. As might be expected, differences in export production between these two models result mainly from differences in vertical mixing intensity (see section 3.2.1). For simulation LBc, the mechanisms of export are more complex so that the link between export production and surface PO_4^{3-} concentrations is not so evident. The primary production is vertically distributed in the euphotic zone, and the export production also depends on the depth of POC production. The deeper that POC production occurs, the less it is regenerated in the first 100 m by grazing or remineralization, and the more it is exported. Thus the maximum in export production in the central and western equatorial Pacific is not due to higher productivity than in the eastern part. Instead, it is explained by a larger vertical extent of production in this region (due to a deep mixed layer) unlike in the east where all production occurs within the top 30 m (due to a shallow mixed layer).

Again, we emphasize that all three of our biogeochemical schemes are phosphate based. They lack limitation by other nutrients such as Fe, N, and Si. They will thus necessarily fail to reproduce many patterns

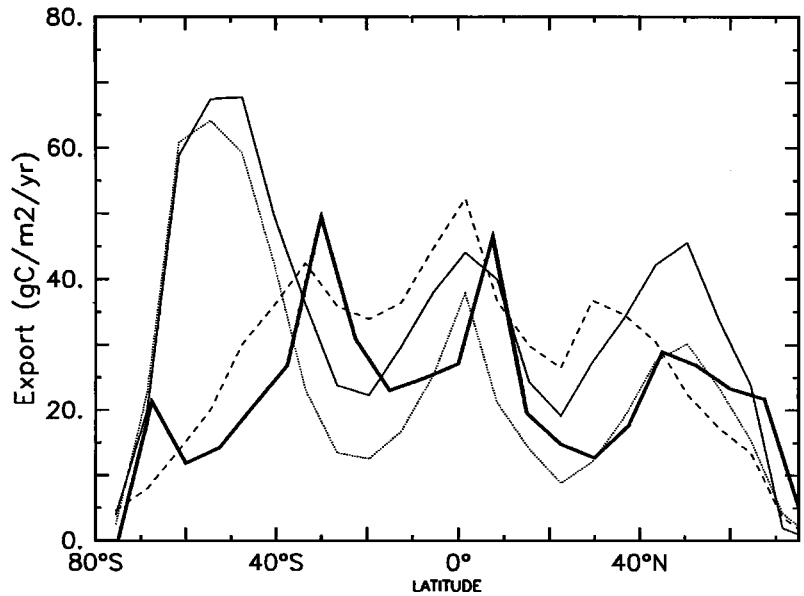

Figure 5. Zonal mean of particulate export production (in $gC\,m^{-2}\,yr^{-1}$) derived from satellite (solid line), and simulated by models LGc (thin, solid line), AGc (thin, dotted line), and LBc (thin, dashed line).

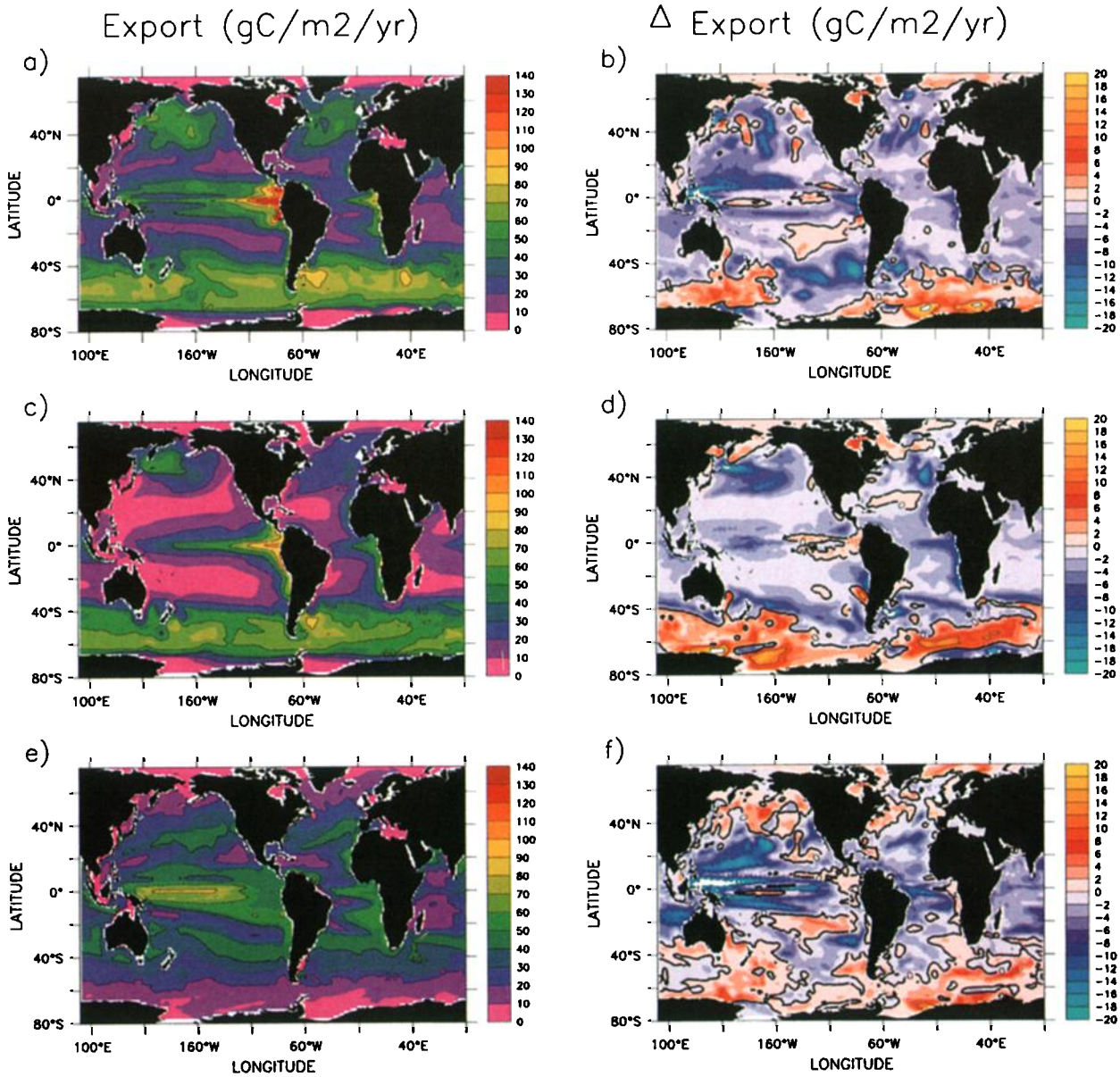

Plate 2. Export Production (in $gC\,m^{-2}\,yr^{-1}$) for (a) LGc, (b) LGs-LGc at $2xCO_2$, (c) AGc, (d) AGs-AGc, (e) LBc, and (f) LBs-LBc.

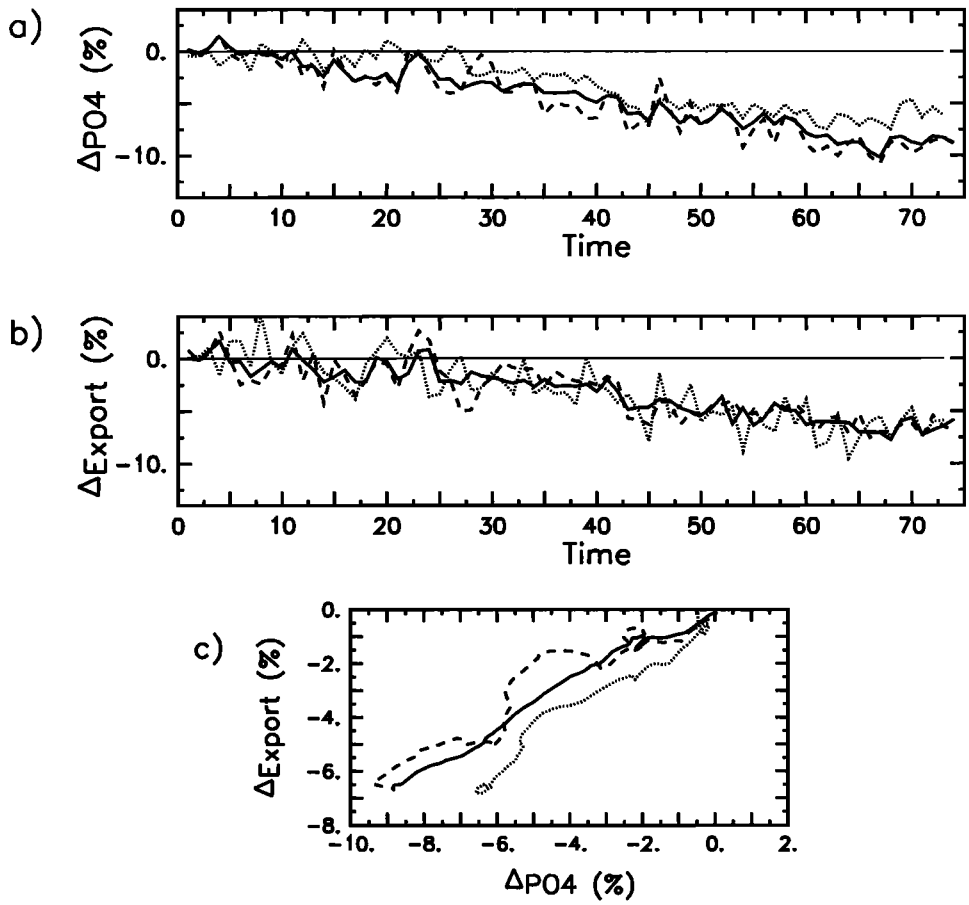

Figure 6. Time series of the relative change (global warming minus control) for (a) surface PO_4^{3-} (LG (solid line), AG (dotted line) and LB (dashed line)), (b) corresponding changes in export production, and (c) the two plotted versus one another.

explained by those missing nutrients, such as in some HNLC regions.

3.3. Biogeochemical Global Warming Runs

Marine productivity in our global warming simulations was substantially altered, relative to the control with both coupled models and both biogeochemical schemes. We focus here on particulate export production because it is the only quantity related to marine productivity that is simulated by the G scheme. Thus we compare our three global warming experiments (AGs, LGs, and LBs).

Models AG, LG, and LB all predict a global decrease in export production at $2xCO_2$, i.e., during years 65-75 (Figure 6b). All three models simulate a reduction of $\sim$ 6% (Table 2). This global decrease in export production is linked to a decrease of similar magnitude of the mean surface phosphate concentration (Figure 6a). Except during the first 20 years of AG simulation, all models show a positive correlation between global export production and global mean surface PO_4^{3-} concentration.

Other diagnostics available with the LB model reveal that the decline in export production is also linked to reductions in total primary production (-8.9%), in surface phytoplankton cell content (-6.3%), and surface chlorophyll content (-8.5%). To look further into the future, we continued our LG run until $4xCO_2$ (at 140 years). Around $3xCO_2$ (year 110), export production is reduced by 11% relative to the control. That lies between the 8 % decrease found by *Maier-Reimer et al.* [1996] and the 15% decrease found by *Matear and Hirst* [1999] in 2100. At $4xCO_2$, export production was reduced by more than 15%.

Zonally, the response of export production to global warming at $2xCO_2$ is surprisingly similar in all models (Figure 7a). There is a a strong opposition between high and low latitudes. All models show that the decline in productivity is principally located in the tropics, reaching -15 to -20%. Furthermore, all models simulate that in subpolar regions (south of 50°S; north of 60°N), export production increases by more than 10%.

In all three models (AG, LG, and LB), reductions in low latitude export production are located similar-

Table 2. Export Production. Control and Impact of Global Warming [a]

	LG		AG		LB	
	Control	Scenario	Control	Scenario	Control	Scenario
High Latitude	0.87	0.91 (+5.1%)	0.87	0.93 (+5.5%)	0.27	0.30 (+12.5%)
Midlatitude	6.5	6.1 (-5.1%)	5.2	4.9 (-4.7%)	4.0	3.9 (-0.5%)
Low Latitude	5.8	5.2 (-10.1%)	3.5	3.1 (-10.9%)	6.8	6.1 (-11.0%)
Total	13.1	12.3 (-6.6%)	9.5	8.9 (-5.9%)	11.1	10.3 (-6.6%)

[a]Given in GtC yr^{-1}.

ily in Indian Ocean, Tropical Atlantic and Western Pacific (Plate 2). Conversely, one of the largest conflicts among models concerns simulated export production in the North Pacific. Between 30° and 60°N, the LB model shows no changes whereas LG and AG predict a 10-20% decrease in export production. Other large conflicts between models occur in the Southern Ocean. The AG model predicts that climate change will induce an increase in export production in the Weddell and the Ross Seas, and even throughout the entire Southern Ocean (up to 20 gC m^{-2} yr^{-1}). Conversely, the LG and LB models predict much patchier changes in export production accross the Southern Ocean: they predict decreases in the Ross Sea and the southeastern Pacific and large increases in the Weddell Sea and the rest of the Southern Ocean.

We were also interested in changes in upwelling and the response of marine productivity, especially in economically important fisheries regions such as off of coastal Peru-Chile and in the equatorial Pacific. A weak

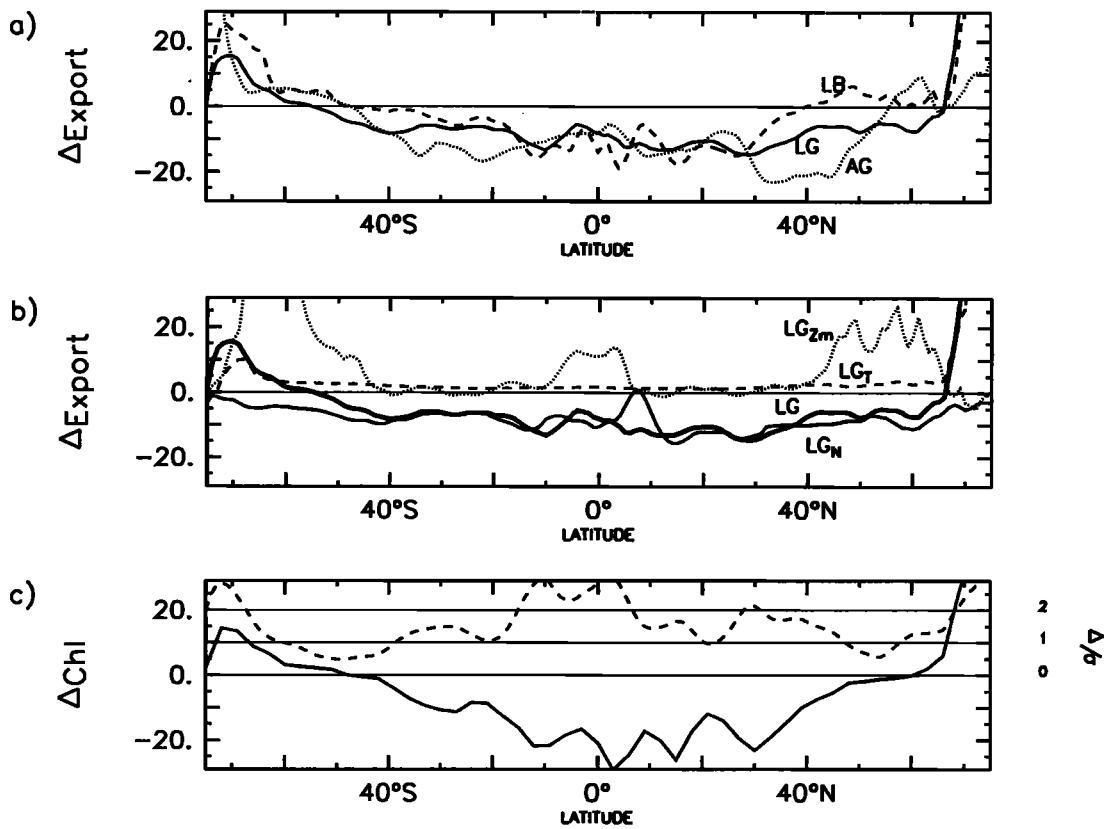

Figure 7. (a) Relative change of the zonal mean of export production (global warming minus control) for the decade of 65-75, simulated by LG (solid line), LB (dashed line) and AG (dotted line); (b) the total relative change (solid line) in LG export production and changes due to thermal LG_T (thin, dashed line), stratification LG_{Zm} (thin, dotted line), and nutrient LG_N (thin, solid line) effects; (c) the relative change of surface chlorophyll from LB (solid line) for the decade 65-75, and the zonal mean of detectability criterion (Δ/σ) for surface chlorophyll (dashed line).

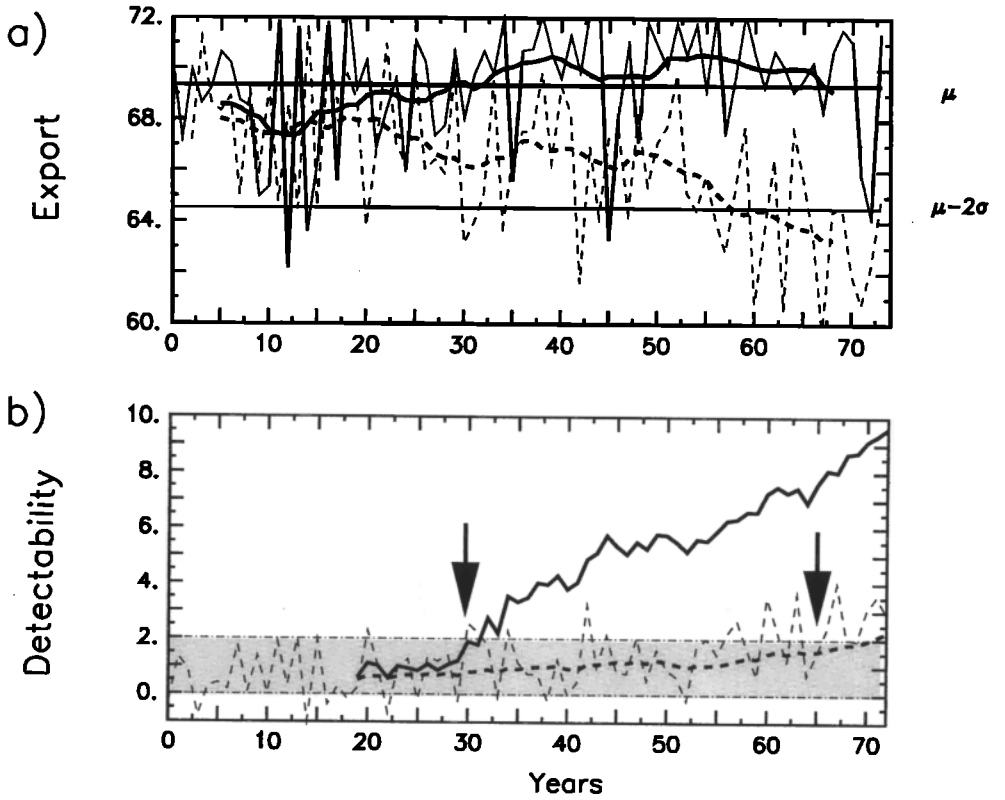

Figure 8. (a) Equatorial Pacific export production ($gC\,m^{-2}\,yr^{-1}$) for LBc (solid line) and LBs (dashed line). Heavy lines are 10-year running means; μ is the mean of LBc; and $(\mu - 2\sigma)$ is the mean minus two times the standard deviation of LBc. (b) Estimation of detectability of export production in the equatorial Pacific with LB model. Comparison of the detectability index DI (heavy, solid line), the ratio Δ/σ (dashed line), and a 20-yr running mean of Δ/σ (thick, dashed line). Within the grey band, there is less than 95% confidence that differences between LBc and LBs are significant.

reduction in upwelling (Figure 2d) leads to decreased nutrient supply in all simulations (nearly -10%). Decreased nutrient supply reduces surface nutrient concentrations, thereby reducing export production by -5 to -15% (Figure 8).

Although the mechanism is simple (less PO_4^{3-}, less export) and can be invoked regionally as well as globally, does it explain all of the simulated changes in marine productivity? Changes in export production and surface PO_4^{3-} are not correlated everywhere (e.g., compare maps of each in Plate 2 and Figure 9). Thus other factors come into play as will be discussed in section 4.

4. Discussion

4.1. Mechanisms

The simplest biogeochemical scheme is rudimentary enough to allow us to separate out the factors that limit export production. In the G scheme, (1) reveals that the change in export production can be separated into changes due to temperature, changes due to light efficiency, and changes due to nutrient supply. Thus we have recomputed export production using monthly-mean fields of temperature, mixed layer depth, and PO_4^{3-} concentrations from both the control experiment and the global warming experiment. By difference we thus quantify the relative contribution of each of the three changes mentionned above (Figure 7b).

On one hand, the decline of surface nutrient supply in LG results from reduced upwelling intensity and reduced wintertime vertical mixing. This decline occurs nearly everywhere, thereby reducing surface PO_4^{3-} concentrations (Figures 9a-9c). Surface PO_4^{3-} drops by up to 0.4 $\mu mol\,L^{-1}$, in the North Pacific, the Southern Ocean, and the west equatorial Pacific. Figure 7b shows that surface PO_4^{3-} reductions drive decreasing productivity in the tropics and midlatitudes.

On the other hand, increased stratification leads to a better photosynthetic efficiency during spring and summer. This effect is most notable in the mid latitudes and high latitudes, where shallowing of the mixed layer occurs earlier in the year and the deepening occurs later

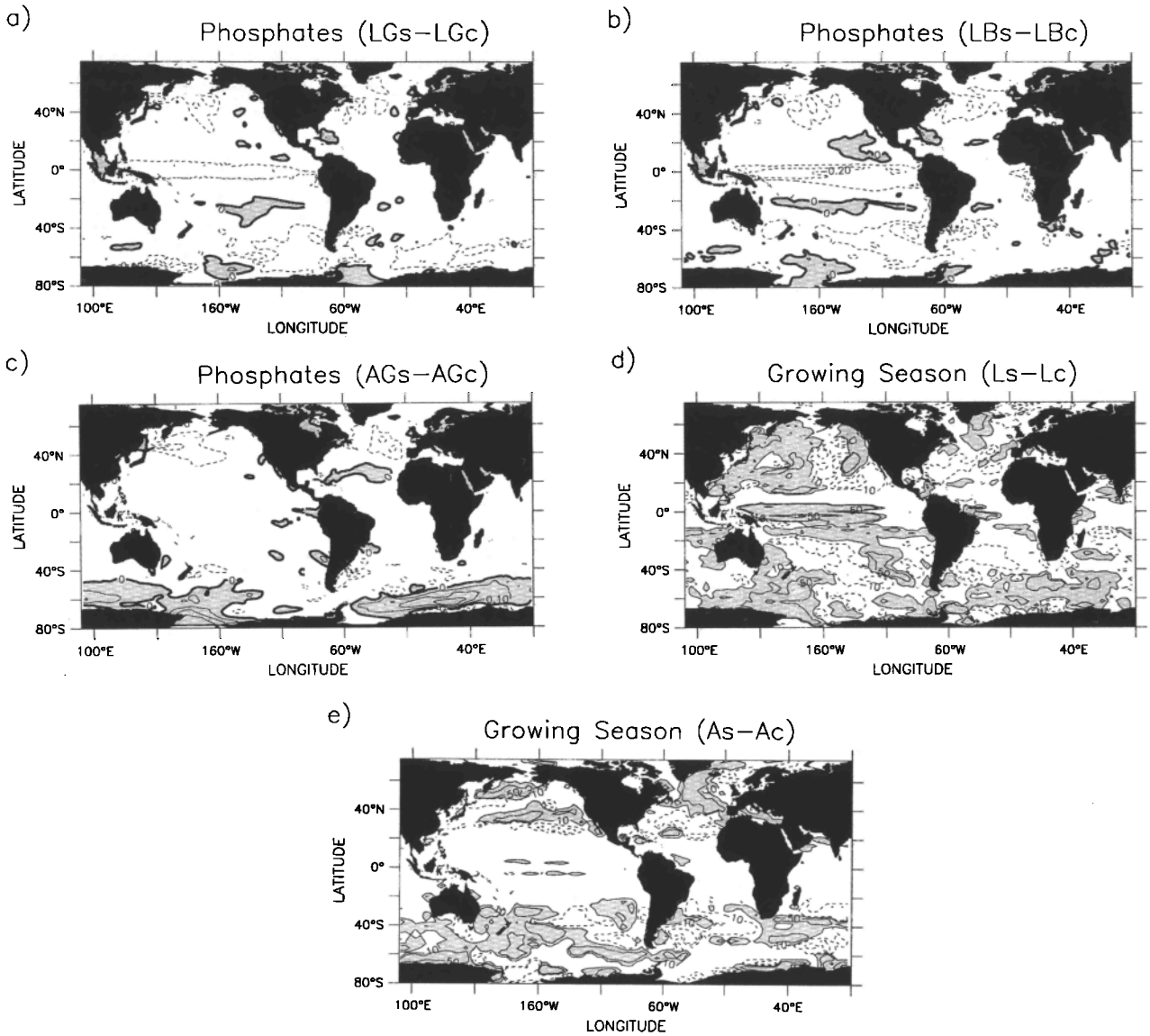

Figure 9. Evolution of surface PO_4^{3-} for the decade 65-75 ($2xCO_2$) for (a) LGs-LGc, (b) LBs-LBc, and (c) AGs-AGc (in μmol L^{-1}, contours are every 0.1 μmol L^{-1} and shaded areas indicate an increase in PO_4^{3-} concentrations). Evolution of the length of the growing season (defined with a mixed layer shallower than 100m) for the decade 65-75 ($2xCO_2$) for (d) Ls-Lc, and (e) As-Ac (in days, contours are -50, -10, 10, and 50, shaded areas indicate an increased growing season by more than 10 days.)

in the global warming simulation relative to the control run Consequently, the growing season length, defined as the period when the light efficiency is reduced by half or less (i.e., $Z_m < 100$ m), tends to expand (Figures 9d and 9e). As an example, in the Southern Ocean (south of 30°S), the length of the growing season increases by $\sim$ 10 days and more than 50 days for several areas at $2xCO_2$ and for both coupled models. These modifications of seasonality and amplitude of the mixed layer depth imply better as well as longer light utilization in the euphotic zone In the LGs model, the positive effect due to a longer growing season reduces the negative effect due to decreased nutrient supply in the equatorial band and even leads to increased export in the high latitudes (Figure 7b). Finally, the third factor, temperature, does not significantly affect modeled export production, except in the very high latitudes (beyond 70°).

Of course, the three limiting factors discussed here are not independent. For instance, changes in surface ocean winter stratification drive changes in surface PO_4^{3-}, changes in surface ocean summer stratification

affect light efficiency and thus the length of the growing season. This simple analysis cannot fully distinguish dynamical from biogeochemical effects. To offer further insight, we provide sensitivity tests with two different coupled dynamical models and two different biogeochemical schemes, thereby illustrating the relative importance of incremental changes in circulation, mixing, and biogeochemistry.

4.2. Sensitivity to Ocean Dynamics

To investigate the sensitivity of our results to the choice of the climate model, we compared climate-change effects in LG and AG. Both models show a similar global decrease of export production, 6.6 and 5.9%, respectively. Furthermore they show generally consistent regional patterns of change. Yet the difference between the high latitudes (increased production) and the low and middle latitudes (decreased production) is larger with AG than with LG. There are also other notable differences, namely in the Southern Ocean.

In the Southern Ocean, stratification increases more in L than in A. In the latter, mixed layer deepens south of 70°S (Figure 3c). Yet both models predict an increase in export production in this region, although for different reasons. In LGc, deep convection limits export production despite high phosphate concentrations. The increased stratification in LGs reduces nutrient supply (Figure 9a), but increases export production due to improved light utilization, i.e., through shallowing of the mixed layer. In AGs, export production is increased relative to AGc because surface phosphate concentration increases south of 60°S (Figure 9c), owing to a deepening of the mixed layer depth in the Weddell and Ross Seas. In AGs, high phosphate concentrations are higher throughout the entire Southern Ocean, thereby increasing export production.

4.3. Sensitivity to the Biogeochemical Model

To investigate the sensitivity of our results to the choice of the biogeochemical scheme, we compared changes in LG and LB. Despite strong discrepancies between control runs, both models produced similar changes in export production. Globally export production decreased by $\sim$ 6% in both models, but this decrease occured mainly in the tropics, whereas export production increased in the high latitudes. The only region where these two models disagree substantially is the North Pacific.

In LG, export production decreases in the North Pacific with global warming, whereas LB shows even a slight increase of export (Plates 2d and 2e). This difference is due to the importance of zooplankton grazing, which LB is able to model explicitly. In the simplistic model LG, only nutrient supply limits productivity in this region. Less wintertime vertical mixing (see mixed layer depth in Figure 10a) in LGs versus LGc reduces the supply of nutrients (Figure 10b) and causes a reduction in export production (Figure 10c). *Frost* [1987] also suggested that zooplankton grazing limits productivity in the North Pacific, an HNLC region. At 170°W, 45°N in this region, the spring bloom in LBc began in April when the mixed layer shoaled rapidly. However, phytoplankton concentrations decreased after May due to increased zooplankton grazing pressure (Figure 10d): in LB, zooplankton grazing limits productivity. Decreased nutrient supply has no effect on export production, which is already limited by grazing. Moreover, the slight increase of export production owing to climate change (LBs-LBc) (Figure 10c) is explained by a longer growing season (less springtime and summertime vertical mixing).

4.4. Limits and Uncertainties

Two major uncertainties are indicated by our sensitivity tests with the AG, LG, and LB simulations. First, reducing uncertainties in ocean dynamics is crucial to be able to properly evaluate climate impact on marine productivity. Such is clearly demonstrated by differences between the two coupled simulations AG and LG. The Southern Ocean is particularly sensitive. In that region, the water column simulated by LGc is weakly stratified and there are large areas of deep convective mixing; in AGc, the water column is much more stratified. The resulting impact of climate change (LGs-LGc versus AGs-AGc) differs dramatically. On the basis of the observed mixed layer depth, it may be that these two simulations would bracket real ocean behavior. However, the link between the present state of the ocean and future changes is not clear. A better representation of the hydrological cycle in the atmosphere is needed to properly simulate ocean dynamics in the Southern Ocean. In the ocean, there have been recent improvements in modeling, for example, parameterization subgrid scale mixing eddies [*Gent et al.*, 1995; *Matear and Hirst*, 1999] and downslope transport which is important for deep-water formation [*Beckmann and Döscher*, 1997]. Ultimately though, improving simulations of Southern Ocean circulation may require much higher resolution and better sea-ice models. Improved simulations of the Southern Ocean physics would improve predictions of changes in marine productivity.

Second, there are regional differences between simulated changes in export production from our two biogeochemical schemes G and B. The more sophisticated scheme B shows that zooplankton grazing can indeed be limiting in some regions and that such process needs to be accounted for under climate change. Other limiting nutrients such as Fe and Si are not accounted for in our models. Changes in the supply of iron, both from above (atmospheric deposition) and below (deep

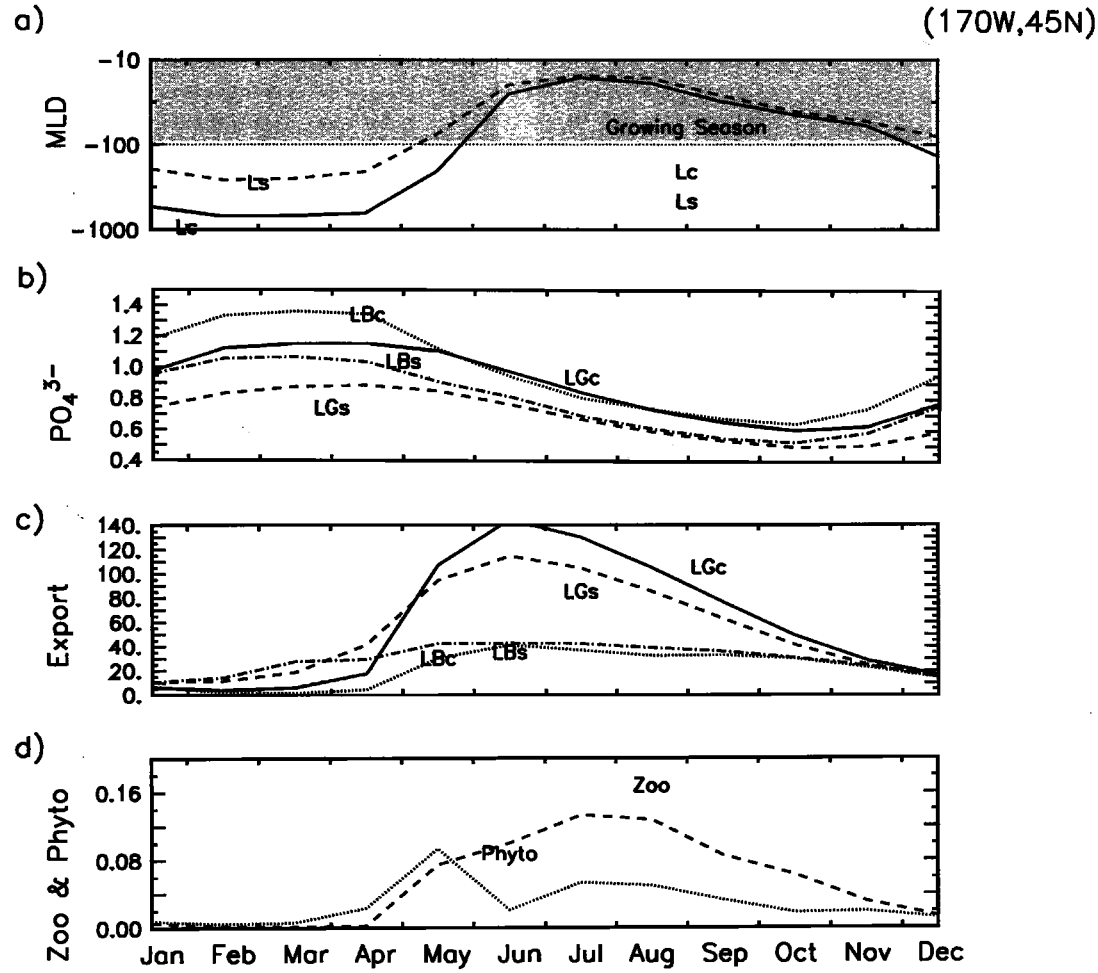

Figure 10. The seasonal cycle at 170°W,45°N (North Pacific) for (a) the mixed layer depth for Lc (solid line) and Ls (dashed line), with the grey shaded area denoting mixed layer depths < 100 m, i.e., which defines the growing season (see text); (b) the mean PO_4^{3-} concentration (μmol L^{-1}) in the upper 50 meters for LGc (solid line), LGs (dashed line), LBc (dotted line), and LBs (dash-dotted line); (c) the export production (gC m^{-2} yr^{-1}) for LGc (solid line), LGs (dashed line), LBc (dotted line), and LBs (dash-dotted line); (d) surface phytoplankton (dotted line) and zooplankton (dash-dotted line) for LBc (mgC L^{-1}).

ocean supply), would alter marine production. Likewise changes in the supply of Si could also be important in some HNLC regions. Nevertheless, using simple phosphates-based biogeochemical schemes would also mimic the effects of change in whatever nutrient supply from below. Indeed, the impact of change in Fe and Si supply from the deep ocean to surface waters is qualitatively accounted for in our models by subsequent changes in PO_4^{3-} supply from the deep ocean (internal forcing). However, changes in atmospheric deposition of iron on the ocean are independant and represent an external forcing. Another inadequacy of our model is that it does not account for the competition between different species of plankton. Species abundance may well change due to climate induced changes in ocean circulation or mixing [*Arrigo et al.*, 1999]. To account for these effects, similar simulations must be made with a more sophisticated biogeochemical scheme.

4.5. Detectability

Besides providing indications of the potential effects of climate change on marine productivity, models can also be used to provide clues about when such changes could be detectable. A key constraint will be continued global monitoring of surface ocean color. Models can diagnose when the regional impact due to climate change surpasses natural interannual variability. For example, we compare the zonal mean of the relative change of chlorophyll ([LBs – LBc]/LBc) for the decade 65-75 with the ratio of change of chlorophyll

to the standard deviation of interannual variability ($[\mathrm{LBs} - \mathrm{LBc}]/\sigma_{\mathrm{LBc}}$) (Figure 7c). It appears that we will have the best chances to detect the effects of climate change on chlorophyll in the tropics and the high latitudes. In those regions at $2\mathrm{xCO_2}$, the impact of climate change is twice as large as the modeled natural interannual variability.

We are also interested in detecting change at the local scale for a transient period. The evolution of export production in the equatorial Pacific, simulated with LBs, shows a rapid decline. This decrease can be followed by the same ratio ($[\mathrm{LBs} - \mathrm{LBc}]/\sigma_{\mathrm{LBc}} = \Delta/\sigma$) as above to estimate the timing of the reduction. This ratio reaches 1 after 30 years and 2 after 60 years (Figure 8a), attesting a significant reduction from the control run (with 70 and 95% confidence level, respectively).

If we integrate information over a longer period, we have a greater constraint than when comparing Δ/σ for just 1 year. A more sensitive criterion is to define a detectability index (DI), based on a Student test, that compares the 20-year running mean of the global warming simulation ($\overline{(X_s)}_{t-20,t}$) to the mean for the entire control run ($\overline{X_c}$).

$$\mathrm{DI}(t) = \frac{|\overline{(X_s)}_{t-20,t} - \overline{(X_c)}|}{s\sqrt{{N_c}^{-1} + {N_s}^{-1}}}, \qquad (2)$$

In this equation, s is the estimated standard deviation from both simulations and N_c and N_s are the number of years in each experiment (75 and 20, respectively). In the LB model for the equatorial Pacific (Figure 8b), the comparison of DI with Δ/σ demonstrates their relative sensitivity and the importance of continuous time series to detect anthopogenic change. When DI reaches 2, simulated export in LGs is significantly different from that in LBc at a 95% confidence level. This criterion is reached after 30 years of simulation, whereas the ratio Δ/σ reaches 2 only after more than 60 years. As a sensitivity test, we can assume that our model underestimates real interannual variability by a factor of 2. Doubling our simulated interanual variability means that DI reaches 2 15 years later, for example, after 45 years of simulation. Thus this detection index even predicts a near future detection of export changes in this region.

5. Conclusion

We have investigated the impact of climate change on marine productivity as induced by a 1% $\mathrm{yr^{-1}}$ $\mathrm{CO_2}$ increase, using two different coupled atmosphere-ocean models and two different biogeochemical schemes.

Generally, our combinations of these models gave similar responses to climate change. At $2\mathrm{xCO_2}$, they all predict a 6% global decrease in export production, and models show opposing changes between the high and low latitudes. Climate-induced changes in the ocean decreased export production by 20% in the low latitudes but increased export production by 30% in the high latitudes. The factors driving this change are revealed by a simplistic analysis with our rudimentory G scheme. Changes in marine export are driven by opposing mechanisms: by reduced nutrient supply (mainly in wintertime) and an increased light efficiency due to a longer growing season that is longer by up to 50 days at $2\mathrm{xCO_2}$. Both changes result from increased stratification in the upper ocean.

Despite such similarities, our sensitivity tests reveal substantial regional discrepancies. Our results depend on the skill of our models to simulate marine productivity, which in turn rely on model skill to simulate ocean circulation. Improvements in both aspects will be necessary to develop greater certainty in such future predictions.

Changes in marine production will impact biogeochemical cycles, such as dimethylsulfide (DMS) and carbon, which in turn will feedback on climate [*Matear and Hirst*, 1999; *Sarmiento et al.*, 1998; *Gabric et al.*, 1998]. Preliminary results of this carbon-climate feedback loop are presented in a corresponding paper (P. Friedlingstein, Positive feedback of the carbon cycle on future climate change, submitted to Geophysical Research Letters, 2000).

We also know that changes in marine production will almost certainly impact higher trophic levels, even though we have yet to include such complications in ocean carbon-cycle models. Predicted changes in key economic fisheries areas (e.g., in the equatorial Pacific and off of coastal Peru and Chile) are large enough to seriously affect human activities. In both coupled models, climate-induced reductions in upwelling lead to reductions in export production of 10-15%. That would exacerbate the present stress on fisheries in those regions due to overfishing.

Our detectability index suggests in the equatorial Pacific that we may be able to distinguish climate-induced reductions in marine productivity from natural variability when atmospheric $p\mathrm{CO_2}$ reaches 450 ppm. To detect those changes it will be necessary to continue present programs to globally monitor ocean color and to establish long-term biogeochemical time series stations in the ocean.

Acknowledgments. We sincerely thank C. Le Quéré, J. Sarmiento and two anonymous reviewers for comments and M-A. Foujols for computing expertise. The computer time was provided by IDRIS (project 990040). This work grew out of collaboration within the IPSL Pole for Modeling, and is supported by PNEDC and PROOF. This is LSCE report 0394.

References

Anderson, L., and J. Sarmiento, Global ocean phosphate and oxygen simulations, *Global Biogeochem. Cycles, 9*, 621–636, 1995.

Antoine, D., J. M. André, and A. Morel, Oceanic primary production, 2, Estimation at global scale from satellite (coastal zone color scanner) chlorophyll, *Global Biogeochem. Cycles, 10*, 57–69, 1996.

Arrigo, K., D. Robinson, D. Worthen, R. Dunbar, G. DiTullio, M. VanWoert, and M.P.Lizotte, Phytoplankton community structure and the drawdown of nutrients and CO_2 in the Southern Ocean, *Science, 283*, 365–367, 1999.

Aumont, O., Étude du cycle naturel du carbone dans un modèle 3D de l'océan mondial, Ph.D. thesis, Univ. Pierre et Marie Curie, Paris, 1998.

Aumont, O., J. Orr, P. Monfray, G. Madec, and E. Maier-Reimer, Nutrient trapping in the equatorial Pacific: the ocean circulation solution, *Global Biogeochem. Cycles, 13*, 351–369, 1999.

Aumont, O., S. Belviso, and P. Monfray, Dimethylsulfoniopropionate (DMSP) and dimethylsulfide (DMS) sea surface distributions simulated from a global 3-D ocean carbon cycle model, *J. of Geophys. Res.*, in press, 2000.

Balkanski, Y., P. Monfray, M. Battle, and M. Heinmann, Ocean primary production derived from satellite data: An evaluation with atmospheric oxygen measurements, *Global Biogeochem. Cycles, 13*, 257–271, 1999.

Barthelet, P., et al., Simulations couplées globales des changements climatiques associés à une augmentation de la teneur atmosphérique en CO_2., *C. R. Acad. Sci. Paris, 326*, 677–684, 1998a.

Barthelet, P., L. Terray, and S. Valcke, Transient CO_2 experiment using the ARPEGE/OPAICE non-flux corrected coupled model., *Geophys. Res. Lett., 25*, 2277–2280, 1998b.

Beckmann, A., and R. Döscher, A method for improved representation of dense water spreading over topography in geopotential-coordinate models, *J. Phys. Oceanogr., 27*, 581–591, 1997.

Berger, W. H., and G. Wefer, Flux of biogenous materials to the sea floor: Open questions, in *Use and Misuse of Seafloor*, edited by K. Hsü and J. Thiede, John Wiley, New-York, 1991.

Blanke, B., and P. Delecluse, Low frequency variability of the tropical Atlantic ocean simulated by a general circulation model with mixed layer physics, *J. Phys. Oceanogr., 23*, 1038–1053, 1993.

Coale, K., et al., A massive phytoplankton bloom induced by an ecosystem-scale iron fertilization experiment in the equatorial Pacific Ocean, *Nature, 383*, 495–501, 1996.

Déqué, M., C. Dreveton, A. Braun, and A. Cariolle, The climate version of ARPEGE/IFS: a contribution to the French community climate modelling, *Clim. Dyn., 10*, 249–266, 1994.

Doney, S. C., D. M. Glover, and R. G. Najjar, A new coupled one-dimensional biological-physical model for the upper ocean: Applications to the JGOFS Bermuda Atlantic Time-series Study (BATS) site, *Deep Sea Res., 43*, 591–624, 1996.

Dugdale, R., and F. Wilkerson, Silicate regulation of new production in the equatorial Pacific upwelling , *Nature, 391*, 270–273, 1998.

Filiberti, M.-A., J.-L. Dufresne, and J.-Y. Grandpeix, Igloo sea-ice model version 1.0, Notes techniques du pole de modelisation, Institut Pierre-Simon Laplace, Paris, France, 1999.

Frost, B. W., Grazing control of phytoplankton stock in the open subarctic Pacific Ocean: A model assessing the role of mesozooplankton, particularly the large calanoid copepodes Neocalanus spp., *Mar. Ecol. Prog. Ser., 39*, 49–68, 1987.

Gabric, A. J., P. H. Whetton, R. Boers, and G. P. Ayers, The impact of simulated climate change on the air-sea flux of dimethylsulphide in the subantarctic southern ocean, *Tellus, Ser. B, 50B*, 388–399, 1998.

Gent, P. R., J. Willebrand, T. J. McDougall, and J. C. McWilliams, Parameterizing eddy-induced tracer transports in ocean circulation models, *J. Phys. Oceanogr., 25*, 463–474, 1995.

Guilyardi, E., and G. Madec, Performance of OPA/ARPEGE-T21 global ocean-atmosphere coupled model, *Clim. Dyn., 13*, 149–165, 1997.

Houghton, J., L. Meira Filho, B. Callander, N. Harris, A. Kattenberg, and K. Maskell, (Eds.), *Climate Change 1995, The Science of Climate Change*, Cambridge Univ. Press, New York, 1996.

Jahnke, R. A., The global ocean flux of particulate organic carbon: Areal distribution and magnitude, *Global Biogeochem. Cycles, 10*, 71–88, 1996.

Joos, F., G.-K. Plattner, T. F. Stocker, and O. M. and A. Schmittner, Global warming and marine carbon cycle feedbacks on future atmospheric CO_2, *Science, 284*, 464–467, 1999.

Lazar, A., G. Madec, and P. Delecluse, A rationalization of the Veronis upwelling/downwelling system and its sensitivity to mixing parameterizations in an idealized OGCM, *J. Phys. Oceanogr.*, in press, 2001.

Le Quéré, C., J. C. Orr, P. Monfray, O. Aumont, and G. Madec, Interannual variability of the oceanic sink of CO_2 from 1979 through 1997, *Global Biogeochem. Cycles, 14*, 1247-1265, 2000.

Levitus, S., Climatological atlas of the world ocean, *Prof. Pap. 13*, Natl. Oceanic and Atmos. Admin., Washington D.C., 1982.

Levitus, S., M. Conkright, J. Reid, R. Najjar, and A. Mantyla, Distribution of nitrate, phosphate and silicate in the world oceans, *Prog. Oceanogr., 31*, 245–273, 1993.

Madec, G., and M. Imbard, A global ocean mesh to overcome the North Pole singularity, *Clim. Dyn., 12*, 381–388, 1996.

Madec, G., P. Delecluse, M. Imbard, and C. Lévy, OPA Version 8.0 Ocean General Circulation model, Reference manual, Laboratoire d'Océanographie Dynamique et de Climatologie, Paris, France, 1997.

Maier-Reimer, E., Geochemical cycles in an ocean general circulation model: preindustrial tracer distributions, *Global Biogeochem. Cycles, 7*, 645–677, 1993.

Maier-Reimer, E., U. Mikolajewicz, and A. Winguth, Future ocean uptake of CO_2: interaction between ocean circulation and biology, *Clim. Dyn., 12*, 711–721, 1996.

Manabe, S., and R. J. Stouffer, Century-scale effects of increased atmospheric CO_2 on the ocean-atmosphere system, *Nature, 364*, 215–218, 1993.

Manabe, S., R. J. Stouffer, M. J. Spelman, and K. Bryan, Transient response of a coupled ocean-atmosphere model to gradual changes of atmospheric CO_2, Part II, Annual mean response, *J. Clim., 4*, 785–818, 1991.

Martin, J. H., G. A. Knauer, D. M. Karl, and W. W. Broenkow, VERTEX: Carbon cycling in the northeast Pacific, *Deep Sea Res., 34*, 267–285, 1987.

Matear, R. J., and A. Hirst, Climate change feedback on the

future oceanic CO_2 uptake, *Tellus, Ser. B, 51B*, 722–733, 1999.

Najjar, R. G., J. L. Sarmiento, and J. R. Toggweiler, Downward transport and fate of organic matter in the ocean: Simulations with a general circulation model, *Global Biogeochem. Cycles, 6*, 45–76, 1992.

Sadourny, R., and K. Laval, January and July performances of the LMD general circulation model, in *New Perspectives in Climate Modeling*, edited by A. Berger, pp. 173–198, Elsevier, New York, 1984.

Sarmiento, J. L., and C. Le Quéré, Oceanic carbon dioxide uptake in a model of century-scale global warming, *Science, 274*, 1346–1350, 1996.

Sarmiento, J. L., T. M. C. Hughes, R. J. Stouffer, and S. Manabe, Simulated response of the ocean carbon cycle to anthropogenic climate warming, *Nature, 393*, 245–249, 1998.

Six, K. D., and E. Maier-Reimer, Effects of plankton dynamics on seasonal carbon fluxes in an ocean general circulation model, *Global Biogeochem. Cycles, 10*, 559–583, 1996.

Suess, E., Particulate organic carbon flux in the ocean-surface productivity and oxygen utilization, *Nature, 288*, 260–263, 1980.

Terray, L., S. Valcke, and A. Piancentini, The OASIS coupler user guide, version 2.3, Centre Européen de Recherche et de Formation Avancée pour le Calcul Scientifique, Toulouse, France, 1999.

Yamanaka, Y., and E. Tajika, The role of the vertical fluxes of particulate organic matter and calcite in the oceanic carbon cycle: studies using an ocean biogeochemical general circulation model, *Global Biogeochem. Cycles, 10*, 361–382, 1996.

O. Aumont, L. Bopp, P. Monfray, and J. C. Orr, Institut Pierre-Simon Laplace/Laboratoire des Sciences du Climat et de l'Environnement, CE Saclay, L'Orme des Merisiers, F-91191 Gif sur Yvette Cedex, France. (aumont@lsce.saclay.cea.fr; bopp@lsce.saclay.cea.fr; monfray@lsce.saclay.cea.fr; orr@lsce.saclay.cea.fr)

J-L. Dufresne and H. LeTreut, Institut Pierre-Simon Laplace /Laboratoire de Météorologie Dynamique du Climat, Université de Paris 6, PO Box 99, 4 Place Jussieu, F-75252 Paris Cedex 05, France. (Jean-Louis. Dufresne@lmd.jussieu.fr; Herve.Letreut@lmd.jussieu.fr)

G. Madec, Institut Pierre-Simon Laplace/Laboratoire d'Océanographie Dynamique et de Climatologie, Université de Paris 6, PO Box 100, 4 Place Jussieu, F-75252 Paris Cedex 05, France. (madec@lodyc.jussieu.fr)

L. Terray, CERFACS, Climate Modelling & Global Change, 42, Avenue Gustave Coriolis, F-31057 Toulouse Cedex, France. (terray@cerfacs.fr)

(Received December 29, 1999; revised May 11, 2000; accepted August 27, 2000.)